Design of a bismuth ferrite nanocomposite in a polysaccharide matrix

G. P. Aleksandrova,[a]★ A. S. Bogomyakov,[b] A. N. Sapozhnikov,[c] and V. I. Ovcharenko[b]

[a]*A. E. Favorsky Irkutsk Institute of Chemistry, Siberian Branch of the Russian Academy of Sciences, 1 ul. Favorskogo, 664033 Irkutsk, Russian Federation. Fax: +7 (395) 241 9346. E-mail: alexa@irioch.irk.ru*

[b]*International Tomography Center, Siberian Branch of the Russian Academy of Sciences, 3a ul. Institutskaya, 630090 Novosibirsk, Russian Federation. Fax: +7 (383) 233 1399. E-mail: Victor.Ovcharenko@tomo.nsc.ru*

[c]*A. P. Vinogradov Institute of Geochemistry, Siberian Branch of the Russian Academy of Sciences, 1a ul. Favorskogo, 664033 Irkutsk, Russian Federation*

Bismuth ferrite nanobiocomposites obtained using a natural polysaccharide were studied. The morphology of new self-organizing nanobiocomposites, which were dispersed in water, was studied, and the sizes of bismuth ferrite nanoparticles were determined and found to vary in the range of 10—45 nm. The temperature dependence of magnetization of the bismuth ferrite-based nanocomposite with spatially separated particles and the dependencies of magnetization on the external magnetic field at temperatures 5 and 320 K were determined.

Key words: nanoparticles, bismuth ferrite, arabinogalactan, magnetic properties.

The preparation and study of new functional materials with tunable magnetic characteristics is of great importance for the development of a scientific foundation for the production of basic objects in nanotechnology, microelectronics, and biomedicine.[1,2] The successful use of nanodispersed magnetic particles for drug biodelivery, visualization of biological specific features at the cellular or even molecular level, development of drugs for magnetic resonance imaging (MRI) and therapeutic hyperthermia[3,4] proves the relevance of research and testing of biological activity *in vitro* and *in vivo*.[1,5,6]

In addition to iron group metals and their oxides, magnetically ordered materials also include complex oxides, namely ferrites, which have a spinel structure. Interest toward ferrites with various compositions is explained by the fact that at negative temperatures these materials have higher magnetic characteristics compared to magnetite, while the principal specific feature of ferrites is the exceptional variability of its magnetic and mechanical characteristics.[7] Nanosized ferrites are promising materials that have the advantages of a nanostructured object.[2] Among magnets, the most popular and in-demand materials are compounds with bismuth ferrite $BiFeO_3$ and other bismuth ferrites having variable composition (BFO), while bismuth ferrites doped with various metals are considered to be some of the best-studied multiferroics, exhibiting complex magnetic (including antiferromagnetic) and electrical properties that depend on the structural specific features of the resulting objects.[8]

The synthesis of magnetic nanoparticles (MNPs), covering a wide range of compositions and tunable sizes, has advanced considerably, especially in the last decade.[3] Methods such as chemical coprecipitation, hydrothermal synthesis, hydrolysis of metal carboxylates in an organic solvent, and aerosolization were developed to obtain nanosized ferrite particles.[1,2,8] New approaches to synthesis were proposed for the preparation of ferrite nanoparticles (NPs) with various morphologies, such as nanocubes, nanowires, thin films, nanoribbons, and nanorods.[9] The sol—gel method is the most popular chemical approach for the preparation of manganese and cobalt ferrite NPs.[10] Monodisperse MNPs with a diameter of up to 20 nm were obtained using their common and relatively non-toxic acetylacetonates as precursors in the presence of 1,2-diols.[11] Ferrite nanoparticles can be synthesized by various modifications of the environmentally friendly coprecipitation of the corresponding precursors, one of which is coprecipitation in the presence of polymer matrices.[12] The synthesis of cobalt and nickel ferrites by coprecipitation of metal chloride precursors in ethylene glycol in the presence of sodium acetate and ethanol-

Published in Russian in *Izvestiya Akademii Nauk. Seriya Khimicheskaya,* No. 7, pp. 1453—1463, July, 2022.

1066-5285/22/7107-1453

amine was studied, and the characteristics of amine-functionalized NPs with average crystallite sizes of 8—10 nm were presented.[13] When obtaining complex ferrites, iron ions Fe^{2+} can be completely or partially substituted with ions of other metals, but only when $Fe^{3+} : (Fe^{2+} + Me^{2+}) = 2 : 1$ or $Fe^{3+} : Me^{2+} = 2 : 1$. Analysis of the obtained results indicates the presence of a pronounced correlation between the magnetic characteristics and the concentrations and types of substituting cations of RBFO samples.[14—16] In the case of bismuth ferrite with high values of magnetic ordering,[17] many studies were carried out to determine the conditions of its preparation both mechanically[18] and using sol—gel processes,[19,20] with the study of phase diagrams, structural, thermal, and other properties of this unique material, however, these studies are often carried out on powders, the main disadvantage of which is the violation of single-phase structure.[8]

As indicated in published works, chemical condensation is considered to be a universal method for synthesizing ferrite NPs, however, an inevitable problem related to NPs is their internal instability over a lengthy period of time. These small particles tend to form agglomerates to reduce the energy related to a high surface area to volume ratio of nanosized particles. Therefore, it is critical to develop coating strategies to chemically improve the stability of MNPs. Unique conditions for the formation of NPs arise when high molecular weight stabilizers adsorbed on the surface of particles with excess energy are used to inhibit excessive particle aggregation. For example, magnetic polymer composites based on polyvinyl butyral with embedded metal MNPs were synthesized.[21] Macromolecules of a natural anionic polysaccharide, sodium alginate, and a synthetic polymer containing polyacrylic acid units can be used as a polymer matrix.[22] We studied the specific features of modifications of Fe_3O_4 MNPs with sizes in the range of 10—30 nm, obtained by precipitation from Fe^{II} and Fe^{III} salt solutions or from the gas phase, using 3-aminopropylsilane and L-lysine. They have more pronounced hydrophilic properties and, therefore, easily form stable aqueous colloidal solutions.[23,24] Chemically obtained NPs can be modified with peptides[25] and amines[26]. Surface modification methods that are required to achieve a high reproducibility and stability of target MNPs also include organic polymer matrices capable of recognizing by biological targets. An example of these biopolymers is the larch polysaccharide arabinogalactan (AG), which is well known for its antioxidant, antimicrobial, and immunostimulatory properties.[27] Previously, biocompatible nanosized magnetite particles in an AG polymer matrix were synthesized,[28] for which the fundamental magnetic characteristics,[29] the effect of energy absorption of an alternating magnetic field with heat release[30] were determined, and their applicability for antianemic therapy was demonstrated.[31] This indicates that MNPs with an AG matrix open up new possibilities for the development of biocompatible contrast agents for MRI.

In this work, we present the experimental aspects of the preparation of nanodispersed BFO in a polysaccharide matrix: their chemical synthesis, the study of their structure and surface, and the investigation of the magnetic properties of the nanocomposites (NCs).

Results and Discussion

Nanodispersed water-soluble bismuth ferrites BFO—AG were prepared using chemical condensation by alkaline co-hydrolysis of bismuth and iron salts in the presence of polysaccharide AG as a matrix stabilizer. The synthesis of NCs based on BFO from precursors was initiated by shifting the pH of the reaction mixture toward the alkaline region by adding a KOH solution to achieve the most complete cocrystallization of metal oxides. Hydrated oxides do not precipitate in the presence of AG in the reaction medium, despite the fact that the pH of precipitation of iron(III) and bismuth(III) hydroxide is 6 and 5, respectively. These processes can be described by Scheme 1, which includes the aqueous hydrolysis of salts and the formation of nanosized hydrated BFO due to increasing pH of the medium (pH 11). The numerous hydroxyl groups of the polysaccharide interact with the forming BFO NPs, and, as a result, the obtained material as a whole has hydrophilic properties, can disperse in water, and, additionally, may have biocompatibility. The polymeric nature of the matrix with a molecular mass M_w of 45.3 kDa[32] ensures the uniform preassigned localization of NPs in a closed spatial branched structure.[29]

The process of formation of bismuth ferrite NPs in an AG matrix was observed by the change of the solution color from transparent yellow to gray-black, as well as using spectrometric monitoring in the UV-Vis region. The electronic spectra of bismuth ferrite—AG NCs show a smooth descending curve with unresolved bands in the region of 250—500 nm and a shoulder at $\lambda = 320$ nm, which differ from the spectra of the starting nitrates. The dynamics of the formation of bismuth ferrite NPs in an aqueous solution of AG, monitored for 2, 4, 6, 10 min, depending on the duration of the reaction, showed that the formation of bismuth ferrite is accompanied by a gradual increase in absorption intensity (1.03, 1.76, 1.89, 2.05) at 320 nm, characteristic for

Scheme 1

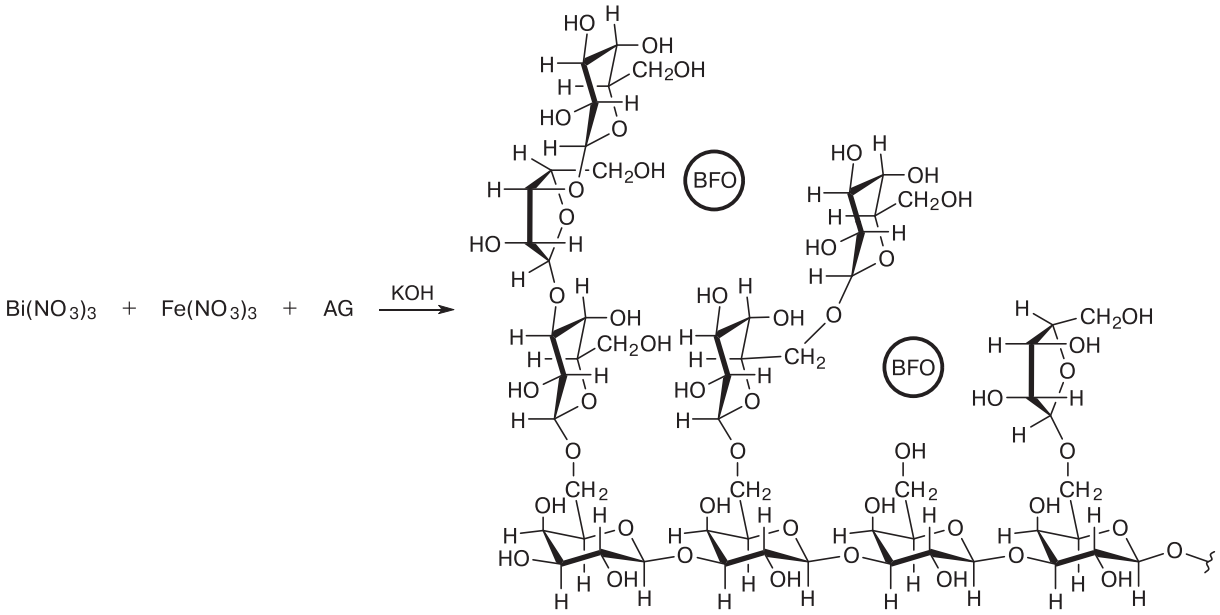

this compound, and the corresponding increase of the intensity of the reaction medium color.

Energy-dispersive analysis determined that bismuth ferrite NCs also contain organic polymeric carbohydrate stabilizers (Fig. 1). The concentrations of bismuth and iron in various NCs varied in the ranges of 11.6—18.6% and 2.8—6.3%, respectively. Changing the composition of the magnetic component of NCs, as well as changing the quantitative ratio magnetic core—polymeric organic matrix, makes it possible to tune their magnetic characteristics within certain limits.

In order to effectively prevent aggregation and precipitation of MNPs, we applied a stabilizing polyol (polysaccharide) coating to the NPs to enable the preparation of injectable solutions that are stable in the long-term or lyophilized powders that are easy to dissolve. Arabinogalactan can ensure the aggregative stability of the resulting NCs, which follows from the

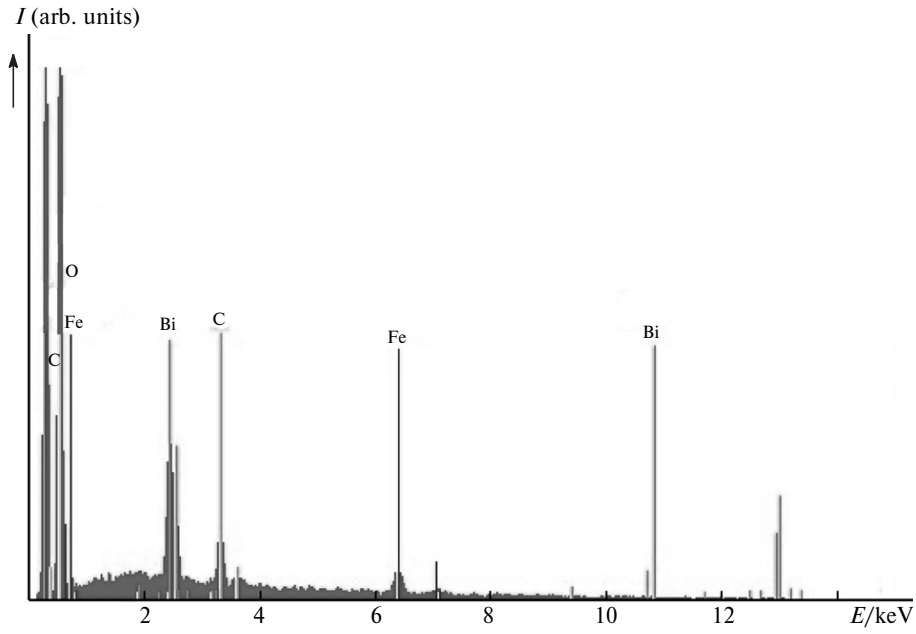

Fig. 1. Energy-dispersive X-ray spectrum of bismuth ferrite-based NCs containing 4.2% Fe and 13.4% Bi.

visual monitoring of their solutions that remain stable for a year. This is probably due to the rather high zeta potential of the starting AG (−23.2 mV), which characterizes the effectiveness of AG as a stabilizer of NPs.

In addition, to achieve the biocompatibility of MNPs with biological targets, their hydrophobic surfaces must be modified. This dual problem was successfully solved by the chosen nature of the coating of NPs with arabinogalactan, which includes galactose monomer units with a high affinity for asialoglycoprotein receptors. Arabinogalactan is a natural polysaccharide polymer, the main chain of which consists predominantly of 1→3-linked β-D-galactopyranose residues, having side branches at C(6), with various chain lengths and branchings. The side chains are represented by 3,6-di-O- and 6-O-substituted β-D-galactopyranose residues and 3-O-substituted β-L-arabinofuranose residues,[33] the ratio of the number of side chain units and galactan core units is 6.1 : 8, which indicates a high degree of branching. Arabinogalactan, as a polysaccharide with a galactan core, is introduced into the hepatocytes of the body as a result of its inherent membranotropy, interacting with them by receptor-mediated endocytosis. The preparation of biocompatible MNPs with AG as a means of delivery to target organs has good prospects. Their principal present and future applications include the development of new nanostructured tools for magnetic theranostics, in particular, for diagnostic imaging of the liver and spleen when administered parenterally, which will improve the detection of liver metastases due to the different rates of absorption of MNPs by healthy and tumor tissues. An animal study of the acute toxicity of AG itself and its metal-containing NCs showed that the average lethal dose (LD_{50}) was 11600—16500 mg kg^{-1}, which made it possible to assign them to class IV low-hazard substances and to consider the potential biocompatibility of such NCs.[27]

The mechanism of surface anchoring of a polymer coating is usually investigated using methods that describe the nature and strength of surface bonding (by hydrogen bonds), as well as the effect of the coating on the structural and magnetic properties of bismuth ferrite. Indeed, surface effects can lead to a decrease of the magnetization of small particles, for example, oxide nanoparticles, compared to bulk materials. To describe the interaction between AG and bismuth ferrite during the formation of NPs, we used IR spectroscopy, which is an effective tool for monitoring the manifestation of functionalization of objects.

The IR spectra of bismuth ferrite—AG NCs show signals characterizing the AG organic matrix (ν/cm^{-1}: 3429 (OH), 2898 (CH_3, CH_2, and CH), 1614 (HOH), 1375, 1220, 1077 (C—O), 886—776 (β-glycosidic bond)) and indicate the presence of an O—Me bond. The differences in the spectra of the starting AG and the obtained NCs, as well as NCs heated at 250 and 300 °C, were observed in the region of 1650—400 cm^{-1}. This region contains absorption bands of the organic matrix and weak bands of characteristic frequencies of vibrations of Fe—O bonds in the range of 530—580 cm^{-1} (see Refs 4, 23—25, 34) and Bi—O bonds in the range of 400—700 cm^{-1}.[35—37] A sharp decrease in the absorption intensity at 1075—1083 cm^{-1} (C—O) in the IR spectra of NCs heated at 250 and 300 °C to an almost complete disappearance of the band is apparently caused by the splitting of C—O bonds during the destruction of the organic matrix accompanying thermal treatment.

For bismuth ferrite obtained under the same conditions of coprecipitation without the presence of AG, intense absorption is observed in the region of 700—400 cm^{-1}, overlapping the ranges of vibrations of Fe—O[4,23—25,34] and Bi—O[35—37] bonds described in published works, since the sample was obtained without additional thermal treatment, which is typically used to form single-phase bismuth ferrites.[38—40] For the same reason, the spectrum contains peaks at 3433 (OH) and 1634 (HOH).

It is difficult to clearly determine the position of the Fe—O and Bi—O bands in the spectrum of bismuth ferrite NCs in an AG matrix, since they overlap with the organic matrix absorption bands in the region of 800—400 cm^{-1}, the content of which is much higher than that of the inorganic component. This was also observed in studies of bismuth ferrites NCs with polyvinylpyrrolidone[40] and organic acid[41] matrices.

Line shifts in the spectral range from 1640 cm^{-1} to 1619—1614 cm^{-1}, related to associated water molecules coordinated with metals and differing in intensity from the lines in the spectrum of the starting AG, are the most sensitive toward the structural features of NCs. The similarity of the IR spectra of the polymer AG and BFO—AG NCs, with the exception of the OH peak intensity, indicates that both AG and BFO—AG NCs have the same basic chemical polymer structure and differ in the degree of self-association with hydrogen bonds.[21]

It is known that in aqueous solutions the surface Fe atoms in iron oxide coordinate with water molecules, which easily dissociate, leaving the iron oxide surface functionalized with hydroxyl groups, capable of interacting with the hydroxyl groups of the polysaccharide. These observations suggest that some AG OH groups form conjugates with MeO, which leads to the disrup-

tion of hydrogen bonds in the starting AG and the formation of new O—Me bonds. An important factor determining the stabilizing ability of AG is, apparently, the favorable size of its chains, which ensures polar interactions (primarily the formation of hydrogen bonds) with iron oxide surfaces. Although a single hydrogen bond is relatively weak, the total energy of all the hydrogen bonds along the entire length of the polysaccharide molecule can be very high due to the large number of hydroxyl groups per macromolecule. Therefore, the studied nanosized bismuth ferrite particles are chemically bound to the biopolymer matrix when placed in this three-dimensional branched structure. The nature of this binding presumably lies in the interaction between the energy-saturated surface of the NPs and the hydroxyl groups of AG. The optimal quantitative ratio of polysaccharide stabilizer and inorganic part of NCs, at which AG prevents coagulation and precipitation of the latter from the aqueous solution, was 3 : 1 for ratios AG : bismuth ferrite equal to 8—2.5 : 1, which indicates the high efficiency of AG as a stabilizer of NPs.

An attempt was made to characterize the obtained BFO—AG NCs using diffraction patterns taken in the range of angles 2θ = 10—60°. A typical diffraction pattern is shown in Fig. 2, *a*. The diffraction pattern *1* has two broad maxima. The first maximum is differentiated as a halo of the AG amorphous phase in the range of angles 2θ = 13—22°. The second maximum is located in the range of angles 2θ = 24—39°, where the reflections of the metal-containing component theoretically should be located, however, there are no narrow peaks of crystalline phases present.

Standards of bismuth ferrites with variable compositions were tested in the analysis, the most common among them were bismuth ferrites $BiFeO_3$, $Bi_2Fe_4O_9$, as well as ferrites with variable compositions $Bi_{24}Fe_2O_{39}$, $Bi_{24}(Bi_{1.04}Fe_{0.84})O_{40}$, $Bi_{3.43}Fe_{0.57}O_6$, however, we observed no correspondence of peak position and intensity of the standards and the experimental diffraction patterns. Previously, NCs with both bismuth oxides and iron oxides with well-crystallized NPs were obtained under similar conditions. The absence of distinct iron oxide peaks in X-ray diffraction pattern *1* in the region of angles 2θ = 30.2, 35.6, 43.1, 57.0, 62.9° in the case of synthesis in the presence of AG using only iron salts as precursors[42] allowed us to infer that in this reaction iron ions interact with bismuth ions with the formation of complex oxide structures, resulting in, according to elemental analysis, a number of bismuth ferrites with variable compositions within the sample. The presence of a halo in diffraction pattern *1* in the region of angles 2θ = 23—36°, where narrow reflections of crystalline

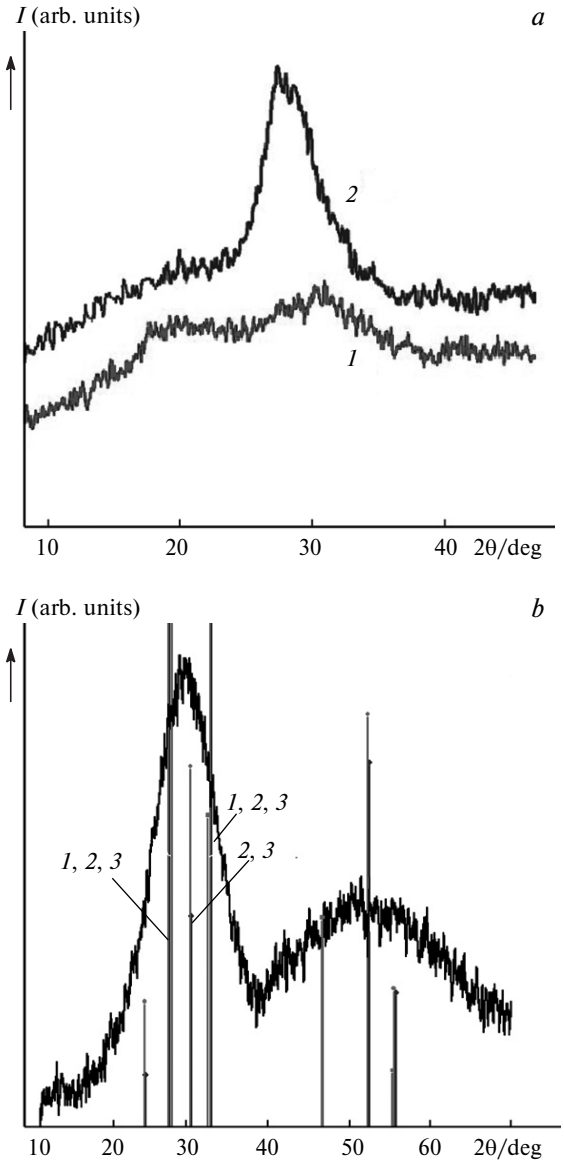

Fig. 2. (*a*) Diffraction pattern of bismuth ferrite NCs in an AG matrix: (*1*) BFO NCs containing 13.4% Bi and 4.2% Fe; (*2*) the same NCs heated at 300 °C. (*b*) Diffraction pattern of bismuth ferrite obtained without the addition of AG, with superimposed reflections of standard ferrites: *1*, $Bi_{3.43}Fe_{0.57}O_6$, *2*, $Bi_{25}Fe_2O_{40}$, *3*, $Bi_{24}(Bi_{1.04}Fe_{0.84})O_{40}$.

phases of the bismuth ferrites being studied should appear, indicates that in this case X-ray amorphous modifications of bismuth ferrites are realized, similar to the existing X-ray amorphous structural states of finely dispersed ferrites.[43]

To confirm that specifically bismuth ferrite is obtained in the reaction, synthesis was carried out under the same coprecipitation conditions without the presence of AG, leading to the precipitation of an inorganic substance from the reaction medium, which was a mix-

ture of ferrites with variable compositions. The X-ray diffraction pattern of the sample is shown in Fig. 2, *b*. Here, the narrow peaks of individual bismuth ferrites are not distinguishable because they begin to overlap due to the broadening of reflections as a result of sample fineness, resulting in a broad peak in the region of angles 2θ = 23—39°. This peak can correspond to bismuth ferrites with variable compositions, including $Bi_{3.43}Fe_{0.57}O_6$ (**1**), $Bi_{25}Fe_2O_{40}$ (**2**), $Bi_{24}(Bi_{1.04}Fe_{0.84})O_{40}$ (**3**), superimposing their strongest reflections in the range of angles 2θ = 27—28°, characteristic of ferrites **1**—**3**, in the range of angles 2θ = 30—31°, corresponding to ferrites **2** and **3**, and in the range of angles 2θ = 32—33°, also characteristic of all three tested bismuth ferrite standards, as well as other weaker reflections of these compounds in the region of larger angles.

Nanoparticles of individual bismuth ferrites are usually obtained only by thermal treatment (500—800 °C) of samples, the composition of which strongly depends on the temperature of synthesis.[44] Heating of BFO—AG NCs at 250 and 300 °C for 2 h, which is recommended in some works on the synthesis of $BiFeO_3$ for structurization, increased the intensity of the maximum in the range of angles 2θ = 23—36°, but did not result in the appearance of narrow reflections of the metal oxide component on the X-ray diffraction pattern (see Fig. 2, *a*, curve *2*). Despite the thermal stability of the starting AG up to 380 °C with temperature increasing at a rate of 10 deg min^{-1},[45] previously determined by TGA, a longer duration of thermal treatment of BFO—AG NCs did not lead to the formation of a pure phase of stoichiometric ferrite, but only contributed to an increase of the inorganic phase content by more than two-fold (from 17.6 to 33.8—40.4%) while maintaining the ratio Bi/Fe at a level of 3.0—3.2, which is intermediate between that of ferrite $BiFeO_3$ (3.73) and ferrite $Bi_2Fe_4O_9$ (1.87). The aforementioned destruction of the organic matrix (evidently a result of the splitting of C—O bonds, detected by a sharp decrease in the intensity of absorption at 1075—1083 cm^{-1} in the IR spectrum to an almost complete disappearance of the band) accompanying the thermal treatment process led to a loss of dispersibility of NCs in water and reduced the value of the object as a biocompatible material.

As established by investigators of ferritic compounds, the system $BiFeO_3$ is characterized by the formation of at least three intermediate phases:[46] $Bi_{25}FeO_{39}$, $BiFeO_3$, and $Bi_2Fe_4O_9$, which form dark brown crystals similar in color to $BiFeO_3$. There is also a large number of substituted bismuth ferrites with structures that include iron atoms with different cationic environments, which influence their spatial structure and magnetic and electrical properties.[47—49] The formation of $BiFeO_3$ is most often reported to be accompanied by secondary phases such as $Bi_2Fe_4O_9$ and $Bi_{25}FeO_{29}$.[50] The widespread synthesis of bismuth ferrite based on BiFeO with a perovskite structure using other structures[50] as bismuth ferrite precursors also results in powders, the main disadvantage of which is the violation of single-phase structure.[8] The conditions under which the synthesized samples were single-phase and did not contain impurity phases, namely, antiferromagnetic $Bi_2Fe_4O_9$ and paramagnetic $Bi_{25}FeO_{39}$, required drastic annealing temperatures and durations,[50,51] which are unacceptable for preserving the biopolymer matrix.

The process of formation of MNPs by condensation consists of nucleation followed by particle growth and has a considerable dependence on the reaction conditions. These two inextricably linked and rapid processes regulate the shape and size of the final product. The study of the surface morphology of the obtained powder nanocomposites makes it possible to determine the specific features of their microstructure. The most typical microstructure of these objects, having a gray-brown color (Fig. 3), are granules that are rather uniform and similar in size (1.3—2.8 μm).

A principal structural parameter of a polymer—MNPs composite material is the uniform distribution of particles in the polymer matrix, since it is well known that the magnetic behavior of a ferrofluid is critically affected by the presence of even a few large particles within the ensemble.[22] Transmission electron microscopy (TEM) was used to study the shape of NPs in the NCs, found to be nearly spherical, and to determine the size of bismuth ferrite NPs, found to vary in the range of 10—45 nm. The branched structure of AG ensures uniform localization of NPs within the matrix and prevents their aggregation (Fig. 4). The size distri-

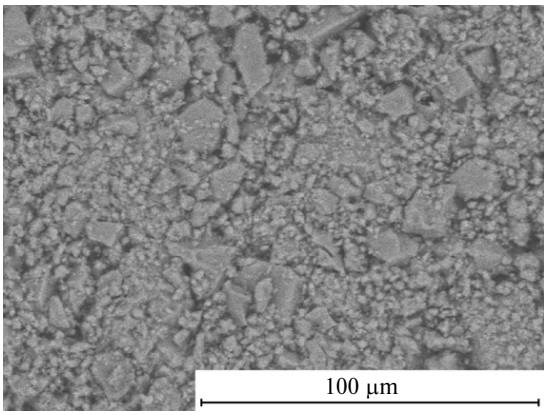

Fig. 3. Surface morphology of bismuth ferrite NCs (the micrograph was obtained by scanning electron microscopy).

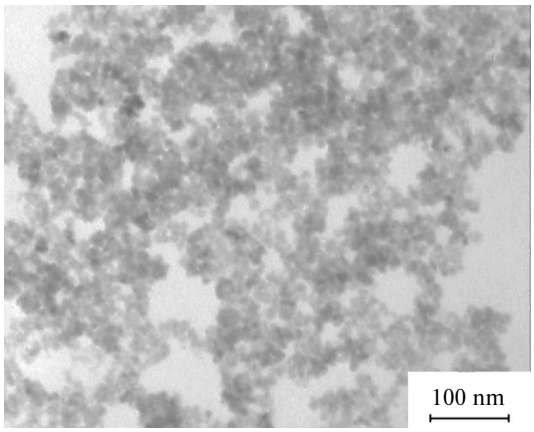

Fig. 4. Typical micrograph (TEM) of bismuth ferrite NPs.

bution of NPs, shown in Fig. 5, *a*, *b*, is monomodal, similar in shape to a Gaussian curve. Statistical calculations confirm that in the case of the synthesized NCs **1** and **3**, the NP sizes increase with inorganic component content within the samples, and the average particle size of the ferrite phase is 23 and 32 nm, respectively. The growth of NPs is limited to this range by the structural features of the AG used as a stabilizer.

The magnetic properties of bismuth ferrite BFO—AG NCs in an AG matrix were studied using a SQUID magnetometer. When studying magnetic materials with MNPs, researchers set apart a large portion of materials consisting of a nonmagnetic organic or inorganic dielectric matrix and magnetic NPs distributed within it. The spatially separated magnetic NPs and the dispersion of their dimensions considerably influence the principal magnetic characteristics of the NCs. The temperature dependencies of the magnetization (M) of the samples in an applied magnetic field of 15 kOe are shown in Fig. 6.

The temperature dependencies of the samples have the same type and reflect an increase in magnetization with a decrease in temperature below 100 K, which is especially pronounced in the low-temperature range of 5—50 K (see Fig. 6, Table 1). In addition, the magne-

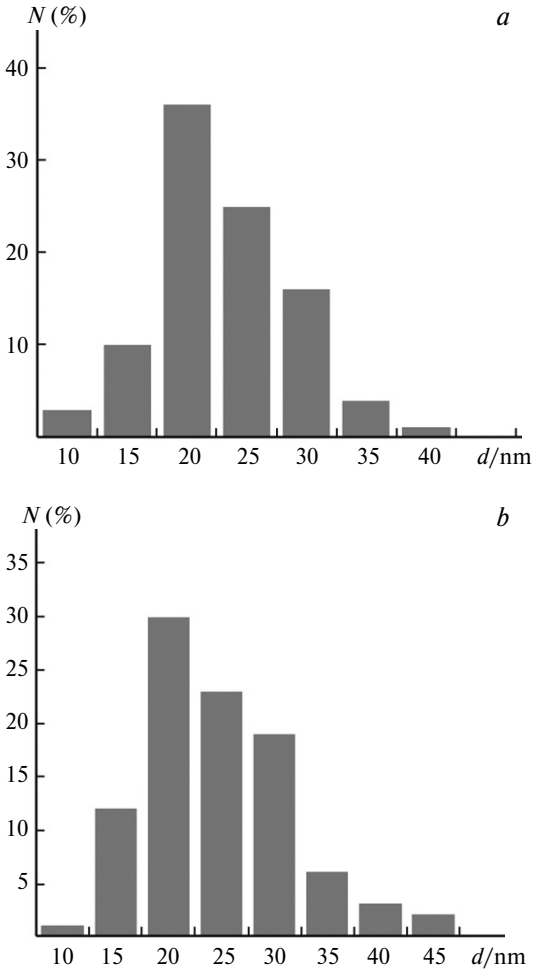

Fig. 5. Size distribution of NPs in NCs containing 2.8% Fe and 11.6% Bi (*a*), 6.3% Fe and 18.6% Bi (*b*); N is the number of particles.

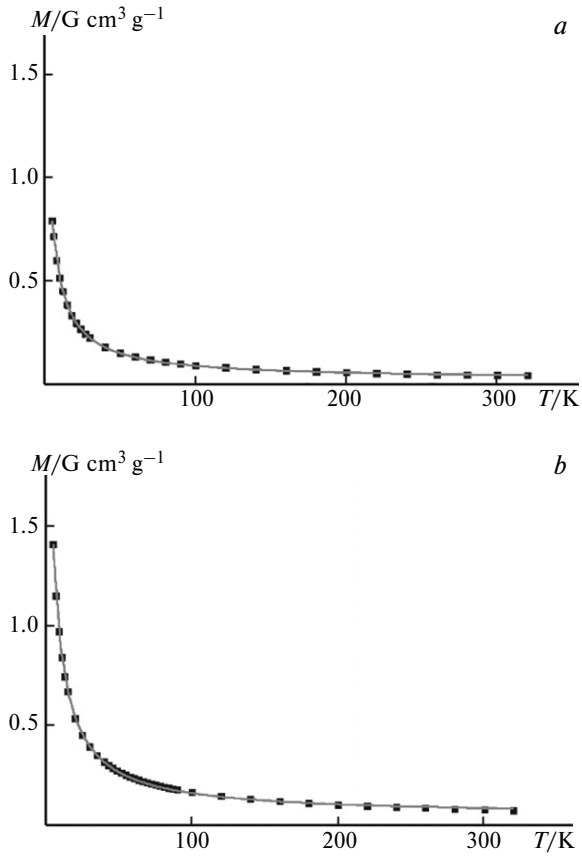

Fig. 6. Temperature dependencies of the magnetization of NCs containing bismuth ferrite NPs in an AG matrix: 2.8% Fe and 11.6% Bi (*a*), 6.3% Fe and 18.6% Bi (*b*).

Table 1. Metal content in MNPs, the ratio MNPs/AG, and the magnetization M of BFO—AG and Fe_3O_4—AG samples in a magnetic field of 15 kOe, measured at temperatures of 5, 50, 300, and 320 K

Sample	Bi	Fe	MNPs/AG	M (in a field of 15 kOe)/G cm^3 g^{-1}			
	%			5 K	50 K	300 K	320 K
BFO—AG	11.6	2.8	1/5.9	0.80	0.16	0.06	0.06
BFO—AG	13.4	4.2	1/4.7	1.27	0.22	0.05	0.05
BFO—AG	18.6	6.3	1/3.0	1.40	0.60	0.03	0.03
Fe_3O_4—AG	—	6.4	1/14.6	104.00	101.00	80.00	78.60

tization in the samples increases from 0.8 to 1.4 G cm^3 g^{-1} in a field of 15 kOe with an increase of Fe and Bi content, and, accordingly, with a change in the quantitative ratio magnetic core—polymeric organic matrix. These dependencies are similar to the effects observed in the case of an increase in the amount of the magnetic component in the polymer matrix, which were first noted in experiments with iron oxide NPs.[30,50,51] When comparing the magnetic characteristics of the obtained BFO—AG with those of the previously studied nanocomposite of AG with magnetite (Fe_3O_4—AG), which has a similar structure and Fe content within the MNPs,[29] it should be noted that its magnetization is much higher over the entire temperature range (see Table. 1), from which it follows that the introduction of bismuth into the composition of MNPs reduces the magnetization of the resulting nanocomposite samples.

The analysis of the temperature dependence of magnetization using the expression $M(T) = M_0 + HC/(T - \Theta)$ makes it possible to isolate the temperature-independent magnetization component M_0 and the contribution of the paramagnetic component, the susceptibility of which obeys the Curie—Weiss law. The optimal values of the parameters M_0, C, and Θ are 0.024 G cm^3 g^{-1}, $4.54 \cdot 10^{-4}$ K cm^3 g^{-1}, and -3.8 K for the sample containing 2.8% Fe and 11.6% Bi, and 0.050 G cm^3 g^{-1}, $7.81 \cdot 10^{-4}$ K cm^3 g^{-1}, and -3.6 K for the sample containing 6.3% Fe and 18.6% Bi. The Curie constant C makes it possible to estimate the amount of Fe in the paramagnetic state. Assuming that Fe in the sample is in the form of Fe^{III} ions in the high-spin state ($S = 5/2$ for a g-factor of 2, C = 4.375 K cm^3 mol^{-1}), ~0.10 mmol g^{-1} of Fe is in the paramagnetic state in the sample containing 2.8% Fe (0.50 mmol g^{-1}) and 0.18 mmol g^{-1} of Fe is in the paramagnetic state in the sample containing 6.3% Fe (1.12 mmol g^{-1}). The values of the Weiss constant Θ indicate the presence of weak antiferromagnetic exchange interactions between the spins of the paramagnetic centers. The temperature-independent component of magnetization M_0 is the sum of the diamagnetism of the AG matrix ($M = \chi_D H < 0$) and the magnetization of the ferromagnet ($M = Ng\mu_B S > 0$), whose contribution is predominant. The M_0 values correspond to ~$8.6 \cdot 10^{-4}$ mmol g^{-1} of Fe in the ferromagnetic state in the case of the sample containing 2.8% Fe (0.50 mmol g^{-1}), and ~$1.8 \cdot 10^{-3}$ mmol g^{-1} of Fe in the ferromagnetic state for the sample containing 6.3% Fe (1.12 mmol g^{-1}). These quantities of Fe in the ferromagnetic state will probably be sufficient for fixating

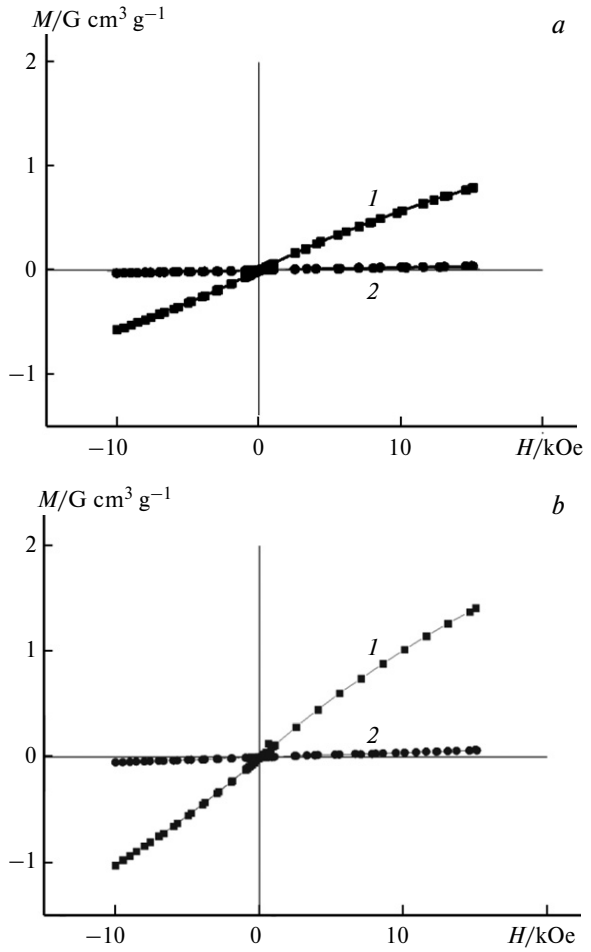

Fig. 7. Field dependencies of the magnetization of bismuth ferrite NCs in an AG matrix containing 2.8% Fe and 11.6% Bi (*a*), 6.3% Fe and 18.6% Bi (*b*) at temperatures of 5 (*1*) and 320 K (*2*).

magnetism in biological objects when these biocompatible NCs are administered parenterally because bismuth ferrite NPs are bound to AG, which can enter the hepatocytes of the body due to its inherent membranotropy.[27] Most of the Fe (80 and 84% of the total Fe content in the samples) is apparently in the antiferromagnetic state.

Field dependencies of magnetization (M) of the samples at 5 and 320 K are shown in Fig. 7. The magnetization of NCs increases slightly with magnetic field strength in the range of 0 to 15 kOe at 320 K, reaching a value of 0.05 G cm^3 g^{-1} (see Fig. 7). The magnetization of bismuth ferrite NCs at low temperatures is much higher than at room temperature and increases almost linearly with applied external magnetic field. In the case of cyclic remagnetization of the studied NCs, the dependence of magnetization on external magnetic field shows no hysteresis, therefore, a considerable portion of the substance in the obtained bismuth ferrite samples is paramagnetic. It was found that the limiting magnetization δ of the samples at 5 K as a function of the magnetic field is in the range of 0.85—1.40 G cm^3 g^{-1} and increases with ferrite content in the samples (see Fig. 7). The magnetization of the previously studied nanomagnetite NCs in an AG matrix, which exhibited a hysteresis loop, is 43.8 G cm^3 g^{-1}, a value that is higher than that of these samples.[29] It is obvious that the substitution of iron ions with bismuth ions in the resulting NPs ensures the formation of a new structure and has a decisive effect on the magnetic characteristics of the samples. Changes in the structure and morphology, nonstoichiometric distortions of the composition lead to changes in the magnetic and ferroelectric properties of nanosized bismuth ferrite (BFO).[51]

Thus, the obtained nanocomposites, the key fragments of which are nanosized bismuth ferrite NPs, uniformly distributed in a polymer matrix, have largely paramagnetic properties both in the low-temperature region and at room temperature. The specificity of the synthesis and the use of a natural polysaccharide as a stabilizing matrix for the forming MNPs provides tunable sizes and a narrow distribution of the dispersion of the resulting particles, determines their long-term aggregative stability, and makes it possible to obtain biocompatible NCs. Changes in the composition and structure of the nanomagnets and the spatial isolation of the NPs that form them lead to a quantitative change of the fundamental magnetic characteristics.

Experimental

The following commercially available reactants were used in the work as the starting compounds without further purification $Bi(NO_3)_3 \cdot 5H_2O$ (reagent grade, Laverna, Russia), $Fe(NO_3)_3 \cdot 9H_2O$ (reagent grade, Khimreaktivsnab, Russia), KOH (reagent grade, Lenreaktiv, Russia).

IR spectra were obtained in the frequency range of 4000—400 cm^{-1} on a Bruker VERTEX 70 instrument in KBr pellets. The optical absorption spectra of aqueous solutions of NCs were recorded with respect to H_2O on a Perkin Elmer Lambda 35 spectrophotometer, cuvette thickness 1 cm. The elemental composition of NCs was determined by X-ray energy-dispersive microanalysis using a Hitachi TM 3000 scanning electron microscope with an SDD Xflash 4304 X-detector and a Flash-2000 ThermoScientific CHNS analyzer. X-ray studies were carried out on a Bruker D8 Advance diffractometer (Cu radiation, a Goebel mirror). To perform phase analysis, diffraction patterns were recorded in the range of 2θ angles from 14 to 80—90°. Crystalline phases were identified by automatically comparing the obtained experimental values of interplanar distances with reference values (DIFFRAC EVA13 software package). Micrographs of bismuth ferrite BFO—AG NPs were obtained on a Leo-906E (Carl Zeiss, Germany) transmission electron microscope with an accelerating voltage of 80 kV. The size distribution of NPs was determined by statistical processing of micrographs. Sample preparation for microscopy was carried out by applying a dilute solution of NCs to a formvar film. The magnetic properties of the samples were studied on a MPMSXL SQUID magnetometer (Quantum Design, USA) in the temperature range of 5—320 K at a magnetic field strength of up to 15 kOe.

Synthesis of NCs. Bismuth ferrite nanobiocomposites (BFO—AG) were synthesized by chemical condensation. A solution containing $Bi(NO_3)_3 \cdot 5H_2O$ (0.2—0.4 mmol) and $Fe(NO_3)_3 \cdot 9H_2O$ (0.2—0.4 mmol) (4 mL) was added to a solution of arabinogalactan (1 g) in water (2 mL) with vigorous stirring, followed by the addition of a 5 M solution of potassium hydroxide to pH 10—11, the reaction mixture was heated at 90 °C for 20 min. The resulting gray-black solution was dialyzed against distilled water for 3 h to remove low molecular weight impurities. The target NC products were isolated from the solution by reprecipitation in ethanol with subsequent washing on the filter and drying. The nanobiocomposites were obtained in high yields (85—95%).

Nanobiocomposites BFO—AG. IR, ν/cm^{-1}: 3429 (OH), 2898 (CH_3, CH_2, CH), 1614 (HOH), 1375, 1220, 1147, 1077 (C—O), 1044, 917, 891—770 (β-glycoside), 776, 705, 700—400 (Bi—O), 590—550 (Fe—O). Found (%): compound **1**: C, 34.4; Bi, 13.4; Fe, 4.2; K, 2.7; O, 45.3; compound **2**: C, 29.5; Bi, 18.6; Fe, 6.3; K, 2.4; O, 41.0; compound **3**: C, 35.0; Bi, 11.6; Fe, 2.8; K, 1.7; O, 48.9.

Individual weighed portions of the dried sample of NC **1** were heated for 2 h at 250 and 300 °C in air. The weight loss after heating at 250 °C was 33%, at 300 °C it was 50%.

Nanocomposite **1** after heating at 250 °C. IR, ν/cm^{-1}: 3431 (OH), 2925 (CH_3, CH_2, CH), 1625 (HOH), 1377, 1281, 1071 (C—O), 782, 545 (Fe—O). Found (%): C, 32.7; Bi, 25.3; Fe, 8.5; K, 4.8; O, 28.8.

Nanocomposite **1** after heating at 300 °C. IR, ν/cm^{-1}: 3431 (OH), 2926 (CH_3, CH_2, CH), 1618 (HOH), 1379, 1282, 1084 (C—O), 790, 537 (Fe—O). Found (%): C, 30.0; Bi, 30.6; Fe, 9.8; K, 5.6; O, 24.1.

Synthesis of bismuth ferrite. A solution containing $Fe(NO_3)_3 \cdot 9H_2O$ (0.4 mmol) (2 mL) was added to a solution of $Bi(NO_3)_3 \cdot 5H_2O$ (0.4 mmol) (2 mL) with vigorous stirring, followed by the addition of a 5 *M* solution of potassium hydroxide to pH 10—11, the reaction mixture was heated at 90 °C for 20 min. The resulting gray-brown solution was collected by filtration, washed with water to remove low molecular weight impurities, and dried. IR, ν/cm^{-1}: 3433(OH), 2922, 2853, 1634 (HOH), 1507, 1456, 1417, 1384, 1340, 1045, 911, 846, 457. Found (%): Bi, 61.2; Fe, 23.1; O, 15.7.

Arabinogalactan (AG) was isolated from an aqueous extract of Siberian larch wood (*Larix sibirica*) and purified by reprecipitation in ethanol. IR, ν/cm^{-1}: 3422 (OH), 2920 (CH_3, CH_2, and CH), 1642 (HOH), 1375; 1216, 1145—1077 (C—O), 886—776 (β-glycoside). Found (%): C, 42.20; H, 6.21; O, 51.59.

The studies were carried out using the facilities of the Baikal Center for Collective Use.

The work was carried out within the framework of the state assignment for research of the Irkutsk Institute of Chemistry, Siberian Branch of the Russian Academy of Sciences, No. 121021000252-84 and with financial support of the Russian Science Foundation (Project No. 18-13-00380).

No human or animal subjects were used in this research.

The authors declare no competing interests.

References

1. R. Qiao, C. Yang, M. Gao, *J. Mater. Chem.*, 2009, **19**, 6274; DOI: 10.1039/B902394A.
2. A. Yu. Gervald, I. A. Gritskova, N. I. Prokopov, *Russ. Chem. Rev.*, 2010, **79**, 219; DOI: 10.1070/RC2010v079n03ABEH004068.
3. M. R. Ibarra, N. G. Khlebtsov, *J. Appl. Phys.*, 2019, **126**, 170401; DOI: 10.1063/1.5130560.
4. J. Mohapatra, A. Mitra, H. Tyagi, D. Bahadur, M. Aslam, *Nanoscale*, 2015, **20**, 9174; DOI: 10.1039/C5NR00055F.
5. D. O. Idisi, J. A. Oke, S. Sarma, S. J. Moloi, S. C. Ray, W. F. Pong, A. M. Strydom, *J. Appl. Phys.*, 2019, **126**, 035301; DOI: 10.1063/1.5099892.
6. A. E. Urusov, A. V. Petrakova, A. V. Zherdev, B. B. Dzantiev, *Nanotechnologies in Russia* (*Int. Ed.*), 2017, **12**, No. 11—12, 471; DOI: 10.1134/S1995078017050135.
7. Z. Boekelheide, J. T. Miller, C. Grüttner, C. L. Dennis, *J. Appl. Phys.*, 2019, **126**, 043903; DOI: 10.1063/1.5094180.
8. A. R. Akbashev, A. R. Kaul, *Russ. Chem. Rev.*, 2011, **80**, 1159; DOI: 10.1070/RC2011v080n12ABEH004239.
9. M. Guan, X. Mu, H. Zhang, Y. Zhang, J. Xua, Q. Li, X. Wang, D. Cao, S. Lia, *J. Appl. Phys.*, 2019, **126**, 064505; DOI: 10.1063/1.5096345.
10. S. Sagadevan, Z. Zaman, C. Rahman, F. Rafiquec, *Mater. Res.*, 2018, **21**, 2; DOI: 10.1590/1980-5373-mr-2016-0533.
11. S. Sun, H. Zeng, D. B. Robinson, S. Raoux, P. M. Rice, S. X. Wang, G. Li, *J. Am. Chem. Soc.*, 2004, **126**, 273; DOI: 10.1021/ja0380852.
12. Ya. Albadi, A. A. Sirotkin, V. G. Semenov, R. Sh. Abiev, V. I. Popkov, *Russ. Chem. Bull.*, 2020, **69**, 1290: DOI: 10.1007/s11172-020-2900-x.
13. N. Momin, A. Deshmukh, S. Radha, *J. Nano Res.*, 2015, **34**, 1; DOI: 10.4028/www.scientific.net/JNanoR.34.
14. I. I. Macoed, A. F. Revinsky, *Phys. Sol. State*, 2015, **57**, 1787; DOI: rep.brsu.by:80/handle/123456789/6193.
15. L. A. Bashkirov, L. I. Krasovskaya, I. A. Velikanova, D. D. Polyko, *Trudy BGTU. No. 3. Khimiya i tekhnologiya neorg. veshchestv* [*Trans. BSTU. No. 3. Chemistry and Technology of Inorg. Compounds*], 2011, No. 3, 43 (in Russian).
16. E. V. Tomina, N. S. Perov, I. Ya. Mittova, Yu. A. Alekhina, O. V. Stekleneva, N. A. Kurkin, *Russ. Chem. Bull.*, 2020, **69**, 941; DOI: 10.1007/s11172-020-2852-1.
17. M. Rohrer, H. Bauer, J. Mintorovitch, M. Requardt, H.-J. Weinmann, *Invest. Radiol.*, 2005, **40**, 715; DOI: 10.1097/01.rli.0000184756.66360.d3.
18. I. Szafraniak-Wiza, B. Andrzejewski, B. Hilczer, *Acta Physica Polonica. Ser. A*, 2014, **126**, 1029; DOI: 10.12693/APhysPolA.126.1029.
19. J. Li, H. He, F. Lü, Y. Duan, D. Song, *MRS Online Proceedings Library*, 2011, **676**, 77; DOI: 10.1557/PROC-676-Y7.7.
20. T. K. Pani, B. Sundaray, *J. Phys.: Condens. Matter*, 2020, **32**, 50, 5802.
21. T. V. Terziyan, A. P. Safronov, I. V. Beketov, A. I. Medvedev, S. F. Armas, G. V. Kurlyandskaya, *Sensors*, 2021, **21**, 8311; DOI: 10.3390/s21248311.
22. V. V. Spiridonov, Yu. A. Antonova, V. S. Kusaya, M. I. Afanasov, S. S. Abramchuk, *Russ. Chem. Bull.*, 2021, **70**, 1675; DOI: 10.1007/s11172-021-3269-1.
23. A. M. Demin, O. F. Kandarakov, A. S. Minin, D. K. Kuznetsov, M. A. Uimin, V. Ya. Shur, A. V. Belyavsky, V. P. Krasnov, *Russ. Chem. Bull.*, 2021, **70**, 1199; DOI: 10.1007/s11172-021-3205-4.
24. A. M. Demin, A. V. Vakhrushev, M. S. Valova, A. S. Minin, D. K. Kuznetsov, M. A. Uimin, V. Ya. Shur, V. P. Krasnov, V. N. Charushin, *Russ. Chem. Bull.*, 2021, **70**, 987; DOI: 10.1007/s11172-021-3177-4.
25. A. M. Demin, A. V. Vakhrushev, A. V. Mekhaev, M. A. Uimin, V. P. Krasnov, *Russ. Chem. Bull.*, 2021, **70**, 449; DOI: 10.1007/s11172-021-3107-5.
26. G. Marinescu, L. Patron, D. C. Culita, C. Neagoe, I. Lepadatu, I. Balint, L. Bessais, C. B. Cizmas, *J. Nanopart. Res.*, 2006, **8**, 1045; DOI: 10.1007/s11051-006-9134-1.
27. V. I. Dubrovina, S. A. Vityazeva, Zh. A. Konovalova, O. V. Yur′eva, T. P. Starovoitova, V. V. Voitkova, G. P. Aleksandrova, V. S. Polovinkina, *Immunomoduliruyushchee deistvie metallosoderzhashchikh nanokompozitov* [*Immunomodulatory Effect of Metal-containing Nanocomposites*}, Megaprint, Irkutsk, 2017, 77 pp. (in Russian).
28. S. A. Medvedeva, G. P. Aleksandrova, L. A. Grishchenko, N. A. Tyukavkina, *Russ. J. Gen. Chem.*, 2002, **72**, 1480; DOI: 10.1023/A:1021654702739.

29. G. P. Aleksandrova, L. A. Grishchenko, A. S. Bogomyakov, B. G. Sukhov, V. I. Ovcharenko, B. A. Trofimov, *Russ. Chem. Bull.*, 2010, **59**, 2318; DOI: 10.1007/s11172-010-0394-7.
30. G. P. Aleksandrova, A. L. Semenov, L. A. Grishchenko, in *Poryadok, besporyadok i svoistva oksidov* [*Order, Disorder and Properties of Oxides*], Rostov-on-Don, 2009, p. 21 (in Russian).
31. S. S. Khutsishvili, G. P. Aleksandrova, T. I. Vakul´skaya, B. G. Sukhov, *IEEE Trans. Magn.,* 2021, **57**, 5200309; DOI: 10.1109/TMAG.2021.3101904.
32. G. P. Aleksandrova, A. S. Boymirzaev, I. V. Klimenkov, B. G. Sukhov, B. A. Trofimov, *Nanotechnologies in Russia* (*Int. Ed.*), 2019, **14**, No. 1—2, 41.
33. S. A. Medvedeva, G. P. Aleksandrova, *Sintez i modifikatsiya polimerov* [*Synthesis and Modification of Polymers*], Khimiya, Moscow, 2003, p. 328 (in Russian).
34. M. I. Ivanovskaya, A. I. Tolstik, D. A. Kotsikau, V. V. Pankov, *Russ. J. Phys. Chem. A*, 2009, **83**, 2081; DOI: 10.1134/S0036024409120140.
35. I. A. Salmani, T. Murtaza, M. Saleem Khan, M. Shahid Khan, *AIP Conf. Proc.*, 2019, **2115**, 030191; DOI: 10.1063/1.5113030.
36. S. R. Dhanya, S. G. Nair, J. Satapathy, N. P. Kumar, *AIP Conf. Proc.*, 2019, **2166**, 020017; DOI: 10.1063/1.5131604.
37. S. Sumathi, V. Lakshmipriya, *J. Mater. Sci: Mater. Electron.*, 2017, **28**, 2795; DOI: 10.1007/s10854-016-5860.
38. P. Roumanille, O. V. Baco-Carles, C. Bonningue, M. Gougeon, B. Duployer, P. Monfraix, H. L. Trong, P. Tailhades, *Inorg. Chem.*, 2017, **56**, 169, 5486; DOI: 10.1021/acs.inorgchem.7b00608.
39. K. Sardar, K. Alia, S. Altaf, M. Sajjad, B. Saleema, L. Akbara, A. Sattar, Z. Alia, S. Ahmed, U. Elahi, E. U. Haq, A. Younus, *J. Nanomater. Biostruct.*, 2020, **15**, No. 1, 51; https://www.chalcogen.ro.
40. O. Amiri, M. R. Mozdianfar, M. Vahid, M. Salavati-Niasari, S. Gholamrezaei, *J. High Temp. Mater. Process.*; DOI: 10.1515/htmp-2015-0045.
41. Y. Hu, L. Fei, Y. Zhang, J. Yuan, Y. Wang, H. Gu, *J. Nanomat.*, 2011, Article ID 797639; DOI: 10.1155/2011/797639.
42. L. P. Feoktistova, A. N. Sapozhnikov, G. P. Aleksandrova, S. A. Medvedeva, L. A. Grishchenko, *Russ. J. Appl. Chem.*, 2002, **75**, 1911; DOI: 10.1023/a:1023318927452.
43. V. I. Popkov, O. V. Almjasheva, M. P. Schmidt, V. V. Gusarov, *Russ. J. Gen. Chem.*, 2015, **85**, 1370; DOI: 10.1134/S107036321506002X.
44. V. M. Denisov, N. V. Belousova, V. P. Zhereb, L. T. Denisova, V. M. Skorikov, *Zh. Sib. Feder. Un-ta. Seriya: Khimiya* [*J. Siberian Fed. Univ. Ser. Chem.*], 2012, **5**, 146 (in Russian).
45. G. P. Aleksandrova, G. F. Prozorova, I. V. Klimenkov, B. G. Sukhov, B. A. Trofimov, *Bull. Russ. Acad. Sci., Physics*, 2016, **80**, 49; DOI: 10.7868/S036767651601004X.
46. V. S. Pokatilov, V. S. Rusakov, A. S. Sigov, A. A. Belik, *Phys. Sol. State*, 2017, **59**, 1535; DOI: 10.21883/FTT.2017.08.44754.438.
47. J. Lin, Z. Guo, M. Li, Q. Lin, K. Huang, Y. He, *J. Appl. Biomater. Funct. Mater.*, 2018, **16**, 93; DOI: 10.1177/2280800017754201.
48. S. Chauhan, M. Arora, P. Sati, S. Chhoker, S. Katyal, M. Kumar, *Ceram. Int.*, 2013, **39**, 6399; DOI: 10.1016/j.ceramint.2013.01.066.
49. V. Srinivas, A. T. Raghavender, K. Vijaya Kumar, *Phys. Res. Int.*, 2016, 4835328; DOI: 10.1155/2016/4835328.
50. C. Baker, S. I. Shah, S. K. Hasanain, *J. Magn. Magn. Mater.*, 2004, **280**, 412; DOI: 10.1016/j.jmmm.2004.03.037.
51. N. Naushin, S. Shahriar, O. Roy, A. Sharif, *J. Eng. Sci.*, 2020, **11**, 123; DOI: 10.3329/jes.v11i1.49555.

Received March 16, 2022;
in revised form June 9, 2022;
accepted June 10, 2022